Complementary Photothermal Heating Effects Observed between Gold Nanorods and Conjugated Infrared-Absorbing Dye Molecules

Kyle Culhane [1,2,*], **Viktoriia Savchuk [1]**, **Anatoliy O. Pinchuk [1,2]** and **Kelly McNear [2]**

1   Department of Physics and Energy Science, University of Colorado Colorado Springs, 1420 Austin Bluffs Park, Colorado Springs, CO 80917, USA
2   UCCS BioFrontiers Center, University of Colorado Colorado Springs, 1420 Austin Bluffs Park, Colorado Springs, CO 80917, USA
*   Correspondence: kculhane@uccs.edu

Abstract: Due to their biocompatibility, ease of surface modification, and heating capabilities, gold nanomaterials are considered excellent candidates for the advancement of photothermal therapy techniques and related applications in cancer treatment. Various morphologies of gold nanomaterials have been shown to heat when exposed to high-powered laser irradiation, especially that which is from the near-infrared (NIR) region. While these lasers work well and are effective, light-emitting diodes (LEDs) may offer a safe and low-powered alternative to these high energy lasers. We investigated the heating capability of NIR-dye conjugated gold nanorods when exposed to an 808 nm LED light source using polyethylene glycol (PEG)-coated gold nanorods as the control. In this way, since the rods exhibited a surface plasmon resonance peak between 795 and 825 nm for both the PEG-coated rods and the dye-conjugated rods, which are fairly close to the frequency of the 530 mW, 850 nm LED light source, we were able to reveal the heating effect of the dye modification. While both morphologies heat when irradiated with the LED light, we demonstrated that the addition of an NIR dye increases the rate of heating and cooling, compared to the PEGylated counterpart. To our knowledge, the complementary effect given by the conjugated NIR-dye has not been previously reported in the literature. The targeting abilities of the NIR-dye combined with the increased heating rate of the modified particles used in this proof-of-concept work suggests that these particles may be exceptional candidates for theranostic applications.

Keywords: metal nanoparticles; infrared light; cancer therapy; surface plasmon resonance

1. Introduction

Cancer is a leading cause of death worldwide, and according to the CDC [1], in 2018, nearly 600,000 people died of cancer in the US alone. Traditional cancer therapies, such as radiation, chemotherapy, and surgery are not only uncomfortable for patients, but can also be costly for both the hospital and those undergoing treatment. The Mayo clinic [2] reports that late effects of radiation and chemotherapy include dental problems, heart problems, infertility, lung disease, and an increased risk of other cancers. Moveover, Yabroff [3] suggests that these potential side effects can be difficult for patients to physically handle and may add secondary costs to their treatment, putting further financial liability on people already bearing the bodily demands of therapy and recovery. It is clear that safe, low-cost, effective alternatives are necessary to mitigate the burden of cancer on our healthcare systems.

Alternative therapies, presented by Lee [4], Wenger [5], Rosenberg [6], and Costello [7], such as laser ablation, have been explored, but are currently still invasive and considered to be a surgical procedure. This can be difficult for patients, particularly those who are elderly or immunocompromised. Additionally, the American Cancer Society [8] reports

that laser treatment has inherent limitations including lack of trained personnel, intense safety precautions, and the need for repeated treatments. Plasmonic nanomaterials, particularly gold nanomaterials, offer a safe, biocompatible, and non-invasive addition to improve current tumor ablation methods by allowing a tumor to be heated via NIR light of wavelengths that can penetrate the skin. Of particular interest are those materials with surface plasmon resonance (SPR) peaks that fall in the near-infrared (NIR) transparency windows (650–1300 nm), as suggested by Pramanik [9], Maestro [10], Zhou [11] and Quintanilla [12], this range is ideal for safely penetrating through biological tissues.

Various morphologies of gold nanomaterials have been shown to heat when irradiated with NIR light. Most recently, Jiang [13] and Alrahili [14,15] explored the heating capabilities and photothermal conversion efficiencies of different morphologies, from size and shape to different surface modifications of gold nanomaterials, when exposed to a 4 W continuous wave 808 nm laser. It was found that morphologies with SPR peaks closer to the frequency of the laser (808 nm) heated quicker and more efficiently than those with off-resonance SPRs. Specifically, we showed that rods with a geometry of 10 × 41 nm with an inherent SPR peak at 808 nm heated well without modification. We also showed that by conjugating 20 nm gold nanospheres (SPR at 524 nm) with an infrared (IR) dye that absorbed at 808 nm their heating efficiency increased by nearly a factor of three. Moreover, IR dyes have been shown to bind to tumors preferentially without the aid of special ligands or other targeting moieties, as shown by Usama [16], Tan [17], Luo [18], C. Zhang [19], E. Zhang [20] and Zhao [21]. By surface functionalizing the gold nanorods with an NIR dye, we can take advantage of these properties to both target and heat tumors effectively. Ultimately, this will allow for the selective heating of malignant tumor cells, while avoiding healthy cells and leaving them intact.

While laser ablation in conjunction with gold nanomaterials is a feasible therapeutic route, we may also consider LED light sources, as they may offer a safe alternative to lasers in photothermal therapy, according to Schüppert [22] and You [23]. Not only are they lower-powered and eye-safe, NIR-LEDs will not require highly trained personnel and are considerably more cost-effective than high-powered lasers. In this work, we aimed to explore how 10 × 41 nm gold nanorods (GNRs) which have been conjugated with a proprietary IR dye (GNRCs), heat when irradiated by a low power (530 mW), 850 nm LED light source. This wavelength was selected as it is within the aforementioned biological transparency window and any observed heating will provide support for future experiments beyond this proof-of-concept work. We explored how the addition of the dye affected the heating rate and the photothermal conversion efficiency when compared to their PEGylated counterparts, used as a control.

2. Materials and Methods

Gold nanorods with dimensions of 10 × 41 nm were purchased from Nanopartz (Loveland, CO, USA). The rods were purchased with functionalized amine-terminated polyethylene glycol (PEG) surfaces, which had a 10 kDa molecular weight PEG group, to allow for the IR 808 nm dye conjugation. The PEGylated gold nanorods were conjugated with a proprietary hepta-cyanine based IR-dye by Lahjavida (Colorado Springs, CO, USA). The PEG groups added approximately 40 nm to each side of the rod, while the dye (approximately 1.1 nm in length) did not contribute significantly to particle size. The presence of the dye molecule on the nanorods after synthesis and purification was confirmed through comparative UV-Vis spectra. N,N-Dimethylformamide (DMF, 99.8%) was purchased from Fisher Scientific. The solutions were irradiated with a 530 mW, 850 nm LED light source (LEDSupply, Randolph, VT, USA) in all experiments presented. The emission spectrum of the LED was measured, and a peak can be observed around 860 nm as shown in Figure A1, found in Appendix A. The temperature of the solution was monitored by an Agilent 34970 A data acquisition system equipped with a k-type thermocouple and using Agilent Benchlink Data Logger 3 software. VWR brand glass cuvettes (path length 1 cm) used for sample measurement were purchased from Fisher Scientific. A power

and energy meter console (PM100D console, ThorLabs) coupled with a photodiode power sensor (S121C, ThorLabs) was used to measure the incident and transmitted power was purchased from ThorLabs.

Three milliliters (3 mL) of the gold nanorod (GNR and GNRC for the PEGylated and IR-conjugated rods, respectively) solution was placed in a glass cuvette and positioned directly in front of the LED, about 5 mm away from the diode. A heatsink was attached to the LED to ensure that residual heat from its operation was not contributing to the heating of the solutions. The solution was continuously stirred to achieve uniform temperature distribution during LED irradiation. The thermocouple sensor was placed in a central position in the cuvette, keeping the surface area in contact with the solution constant between experiments. To show that the solvent did not contribute to the heating of our system, a control experiment was performed. In this, the pure solvents of the GNRs and GNRCs, ultrapure water (UPH$_2$O) and N,N-Dimethylformamide (DMF), respectively, were each added to the cuvette individually and their temperature profiles measured under identical irradiation conditions. During LED irradiation, a negligible temperature increase in the pure solvent was observed, and therefore, we concluded that the gold nanorods were responsible for the temperature changes of the solution (Figure A2).

For the temperature profile measurements, the stock solutions (optical density of 0.8) as well as the solvents, water and DMF, were investigated. The solutions were irradiated until an equilibrium was reached (T_{max}) before the LED was turned off (~2500 s) and then were allowed to cool to room temperature. For the concentration dependence measurements, we explored three different dilutions, including 1:2.5, 1:5, and 1:10. Each solution was irradiated for a total of 1000 s and the temperature was monitored for the duration of the experiment. Each experiment was run in triplicate to ensure reproducibility of the results. A schematic of the experimental set up is shown in Figure 1.
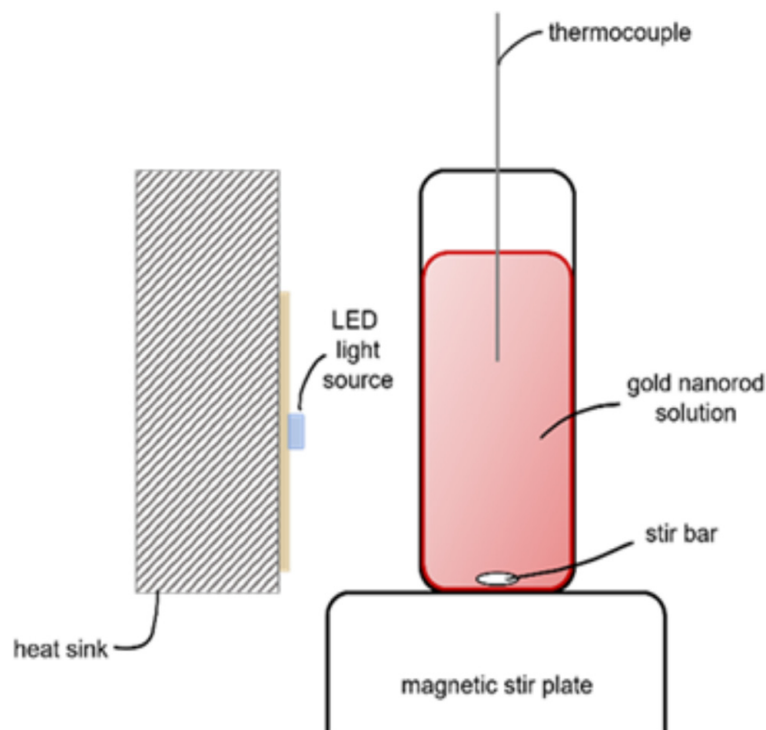
Figure 1. Experimental set up for the heating of a gold nanorod solution via LED. The cuvette was placed about 5 mm from the light source and a stir bar was employed to ensure an even temperature gradient. The thermocouple was positioned in such a way that it was not in the beam path of the LED and the area of its surface in contact with the solution was held constant between experiments.

3. Results

3.1. Photothermal Conversion Efficiency Theory and Calculations

Due to the plasmonic nature of the gold nanorod solutions, irradiation of these solutions with LED light leads to a change in the thermal energy. In general, this can be rationalized by considering Joule heating, or similar effects, in the metal nanoparticle during plasmon oscillations. Following from Jiang [13], Alrahili [14] and Jauffred [24], the thermal energy and temperature change can be expressed from the energy balance between the heat given to the system by the light absorbing nanorods, (Q_{in}), and the heat dissipated from the system to the surrounding environment, (Q_{out}),

$$\sum_i m_i C_i \frac{dT}{dt} = Q_{in} - Q_{out} \tag{1}$$

where m_i and C_i are the mass and specific heat capacity of the individual components in the system, respectively, T is the temperature of the solution, and t is time. For the gold nanorod solutions used in the experiments presented here, the mass of GNRs (about 0.000126 g) is significantly less than that of solvent (2.999 g for water and 2.847 g for DMF), and the heat capacity of gold (0.129 J g^{-1} K^{-1}) is also much smaller than that of the solvents (4.18 J g^{-1} K^{-1} for water and 2.03 J g^{-1} K^{-1}) [13]; therefore, when considering the summation of all individual components, the solvent is the primary contributor to solution's heat capacity. The input heat that is absorbed by the gold nanorods can be described as,

$$Q_{in} = (I_0 - I_{tr})\eta \tag{2}$$

where I_0 is the incident LED intensity, I_{tr} is the intensity of LED light transmitted through the gold nanorod solution, and η is the photothermal conversion efficiency. The heat dissipating from the system to the surroundings can be defined as,

$$Q_{out} = hS(T(t) - T_0) \tag{3}$$

where h is the heat transfer coefficient, S is the surface area of the cuvette, $T(t)$ is the temperature at time t, and T_0 is the initial room temperature at ambient conditions.

Since the volume fraction of the GNRs and GNRCs is small compared to the volume of solvent, we can assume that only the mass and heat capacity of solvent will play a role in our calculations. From consideration of Equations (2) and (3), along with employment of the mass and heat capacity of the solvent, Equation (1) can be written as,

$$\frac{d\Delta T}{dt} = \frac{(I_0 - I_{tr})}{m_s C_s}\eta - B\Delta T \tag{4}$$

where m_s and C_s are the mass and specific heat capacity of the solvent, respectively. Here, we define ΔT as the change in temperature $(T(t) - T_0)$. Additionally, $B = \frac{hS}{m_s C_s}$ defines the rate constant of heat dissipation, which can be determined by exponentially fitting the curve of the temperature profile after the LED has been turned off. In this regime, where the LED is off, $(I_0 - I_{tr}) = 0$, and thus Equation (4) can be reduced to

$$T(t) = T_0 + (T_{max} - T_0)\, exp(-Bt) \tag{5}$$

where the initial condition of the LED turned off corresponded to $t = 0$, and at this point, we have the maximum temperature, T_{max}.

At thermal equilibrium, the temperature is constant and $Q_{in} = Q_{out}$. Therefore, we can now rearrange Equation (4) to find the photothermal conversion efficiency, η,

$$\eta = \frac{(T_{max} - T_0)}{(I_0 - I_{tr})} m_s C_s B \tag{6}$$

Finally, using the η found in Equation (6), we can determine the theoretical temperature change of the gold nanorod solution when the LED is on (during heating experiments),

$$T(t) = T_0 + \frac{(I_0 - I_{tr})}{m_w C_w B} \eta \, (1 - expexp \, (-Bt) \,), \tag{7}$$

3.2. Experimental Determination of Photothermal Conversion Efficiencies

The heat dissipation coefficient, B, must be determined experimentally for each system under investigation. Figure 2 shows a fit of the experimental cooling data (after the LED was turned off), where the slope of this exponential was used to determine the B-values for our samples.
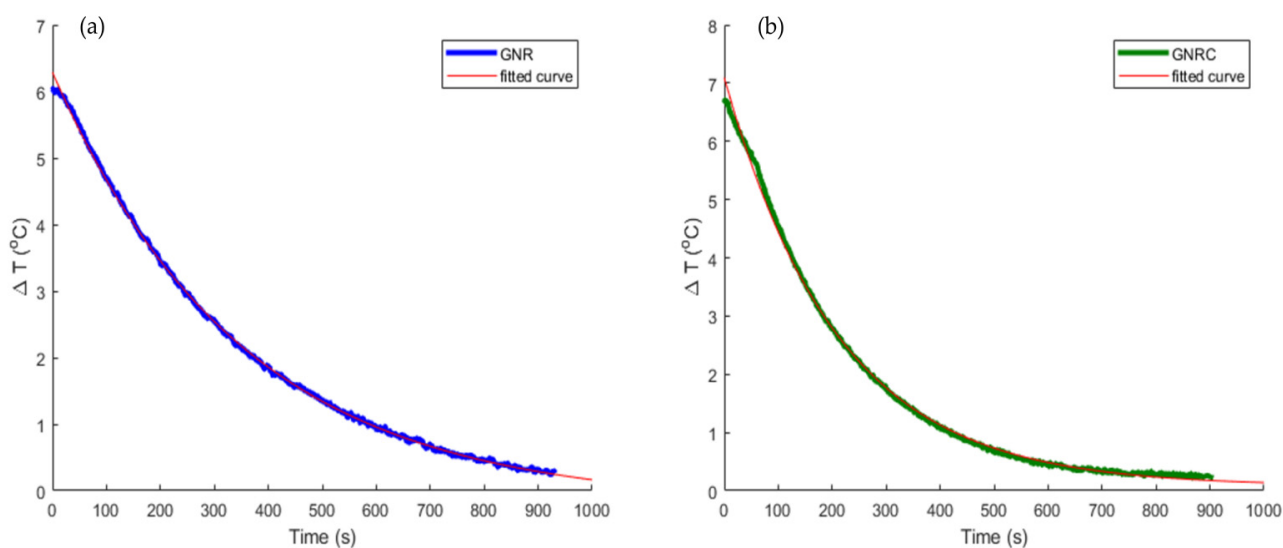
Figure 2. Experimental determination of heat dissipation coefficient, *B*, for use in obtaining theoretical heating profiles and photothermal conversion efficiencies. (**a**) PEGylated GNR sample (determined rate of heat dissipation = $2.87 \times 10^{-3} \text{ s}^{-1}$) and (**b**) IR-dye conjugated GNR sample (determined rate of heat dissipation = $4.75 \times 10^{-3} \text{ s}^{-1}$).

Using these experimentally determined values for the heat dissipation coefficient, along with other parameters matched to experiment, a theoretical heating profile was constructed for a modeled system of particles (Figure 3). Specifically, we plotted the theoretical heating profile for the GNR solution, as these particles' absorption cross section can be determined form Mie theory and can be used to establish the value of Q_{in}. Since Mie theory is typically employed for spherical particles, we used an equivalent radius, R_{eq}, for the 10×41 nm particles to estimate the volume of a spheroid [25,26].

$$R_{eq} = \left(\frac{3V}{4\pi} \right)^{\frac{1}{3}} \tag{8}$$

However, for the dye-conjugated counterparts, Mie theory is not appropriate to use and, therefore, not presented in this work. This was due to a number of assumptions that would need to be made, including the size of the dye, distance of the dye from the rod, as well as number of dye molecules present on the surface of the rod which are beyond the scope of this work. The theoretical temperature profile was, therefore, only constructed for the GNRs, yet it still fits quite well with our experimental data, as seen in Figure 3.

The experimental photothermal conversion efficiency was also calculated by using Equation (6) shown in the previous section. The volume of solution used in the temperature profile experiments was 3 mL and the reported heat capacities of 4.184 J/g °C and 2.030 J/g °C for water and DMF, respectively, were employed for calculations. Using the

ThorLabs power and energy meter console with the photodiode power sensor, the incident power density of the LED was measured to be 0.500 W at the front face of the cuvette and the transmitted power density was measured to be 0.100 W after interacting with the gold nanorod solutions, meaning that the solution absorbed 0.400 W of the incident power. The B values (heat dissipation), calculated from the slope of the cooling portion of the temperature profile curve, were found to be 2.87×10^{-3} s^{-1} and 4.75×10^{-3} s^{-1} for the GNRs and GNRCs, respectively, as shown in Figure 2. From these values, the experimental photothermal conversion efficiency was determined through Equation (6) and calculated to be 50% for the GNRCs and 55% for their unconjugated counterparts. Although it is apparent that the addition of the IR dye did not have much effect on the photothermal conversion efficiency, we must also consider the solvent's characteristics. As reported by Jiang et al. [13], it is important to note that the solvent may play a role in the heat dissipation of the GNRCs, which may in turn impact the B values found from the slope of the line in Figure 2. For comparison, the B value determined for water was 3.26×10^{-3} s^{-1}, and for DMF, it was 3.73×10^{-3} s^{-1}. In contrast to these relatively similar B values fit from the pure solvent data, the GNRC sample exhibited a significantly faster rate of heat dissipation. Moreover, the heating rate over the first 20 s was found to be 0.016 and 0.023 °C/s for the GNRs and GNRCs, respectively, which is also a substantial increase due to the conjugation of the dye. Analysis of the specific mechanisms involved with this behavior was beyond the scope of the work presented here and is a subject of continued investigation.
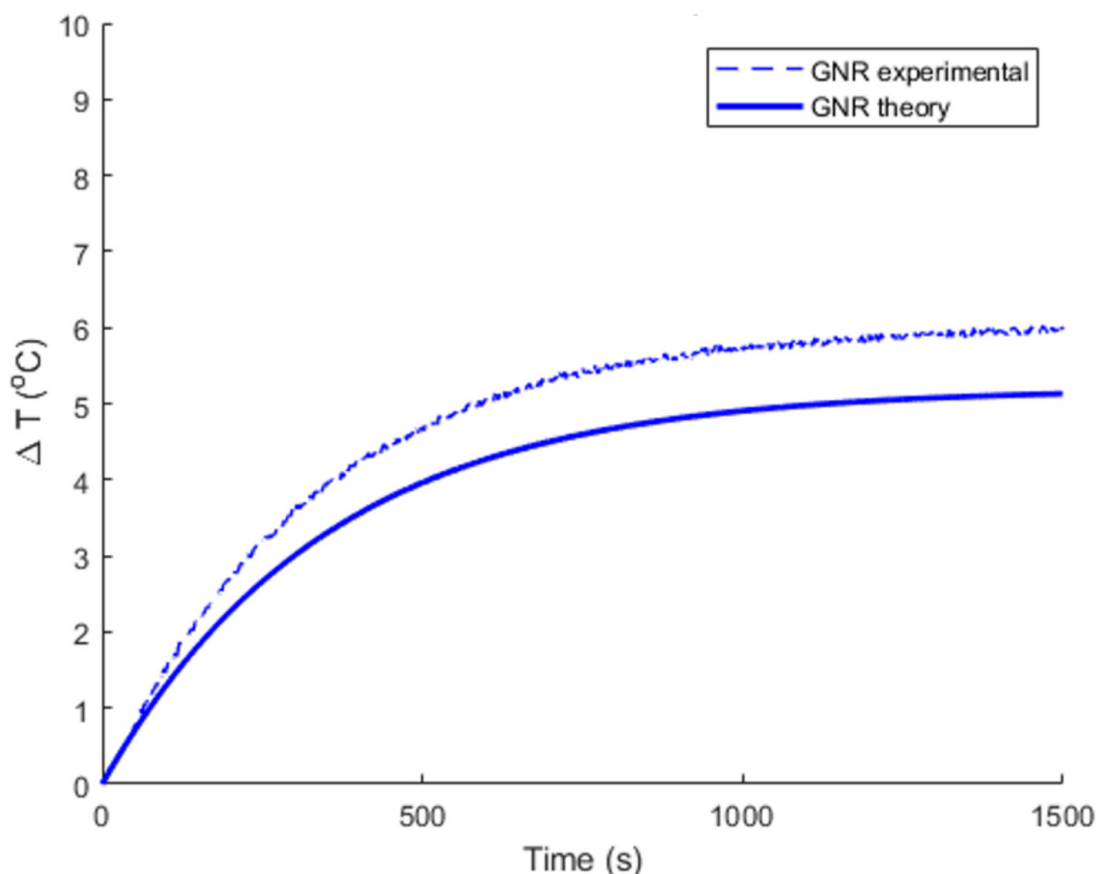
Figure 3. Comparison of theoretically (solid, from Equation (7)) and experimentally (dashed) determined temperature changes for the GNRs. Experimental and theoretical temperature change was determined to be 6.12 and 5.14 °C, respectively.

3.3. LED Heating of the Gold Nanorods and Gold Nanorod Conjugates

For this study, we investigated 10×41 nm PEGylated gold nanorods, as well as their IR dye conjugated counterparts, GNRs and GNRCs, respectively. The gold nanorods were

characterized by UV-Vis spectrometry (PerkinElmer Lamba 1050) to determine the location of the SPR peaks of the solutions as shown in Figure 4. The GNRs exhibit two SPR peaks, which arise from the transverse and longitudinal collective coherent oscillations of the conduction electrons, resulting in a weak peak in the short wavelength range and a strong peak in the longer wavelength range. Since our LED has a wavelength of 850 nm and the first NIR window is in the 700–900 nm range, we were interested in the strong peak which occurs at 794 nm for the GNRs and 822 nm for the GNRCs. To this end, the OD of the solutions was matched at around 0.8 in this regime.
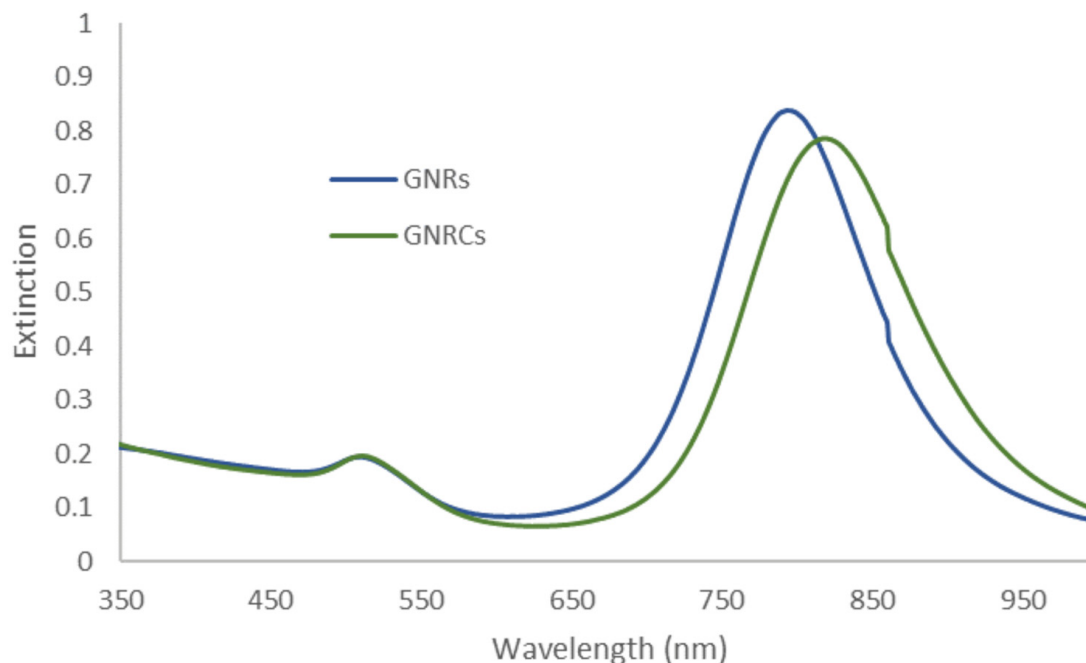
Figure 4. Extinction spectra showing the matched OD of the GNR and GNRC samples at about 520 nm. At the wavelength of interest, the OD of the samples is around 0.8.

The surface-modification of the gold nanorods was shown to play a role in the heating rate of these solutions, as seen in Figure 5. On average, the temperature change of the GNRs was found to be 6.12 °C, and the temperature change of the GNRCs was found to be 7.28 °C. While this is not a substantial difference between the two solutions, the GNRCs clearly reach equilibrium quicker than their unconjugated counterparts and the rate of heating between the two solutions was found to be 44% higher for the GNRCs than the GNRs alone. As the gold nanorods are identical in composition apart from the addition of the dye in the GNRCs, these observations suggest that the addition of the dye plays a role in the overall heat transfer capabilities of the gold nanorods. For additional temperature analysis, including that of the solvents, see Figures A2 and A3 in Appendix A.

As expected, concentration also plays a role in the heating capabilities of the gold nanorod solutions. As we decrease the overall concentration of gold present in the solution through dilution, the temperature change decreases, accordingly, as seen in Figure 6. The stock solution of the GNRs, as provided by Nanohybrids, had a reported concentration of 7.4×10^{11} rods/mL at OD 1. Since the solutions were matched to have an OD around 0.8, the starting concentration of the solutions was calculated to be 5.92×10^{11} rods/mL. To investigate the concentration dependence, we diluted by a factor of 2.5, 5, and 10, resulting in concentrations of 2.37×10^{11}, 1.18×10^{11}, and 5.92×10^{10} rods/mL, respectively. When the solutions are diluted by a factor of 2.5, the change in temperature is 3.62 °C for the GNRs and 4.06 °C for the GNRCs. When diluted by 5, the temperature change is 2.68 °C for the GNRs and 3.43 °C for the GNRCs. Finally, when diluted by a factor of 10, the temperature change is 1.3 °C for the GNRs and 2.40 °C for the GNRCs. This trend is expected as

with each dilution, the predominant component responsible becomes overwhelmingly the solvent, which was shown to not contribute significantly to heating. We also theoretically calculated the temperature change for the various concentrations of the GNRs (Figure 7) and again, the theory matches fairly well with the experimental values.
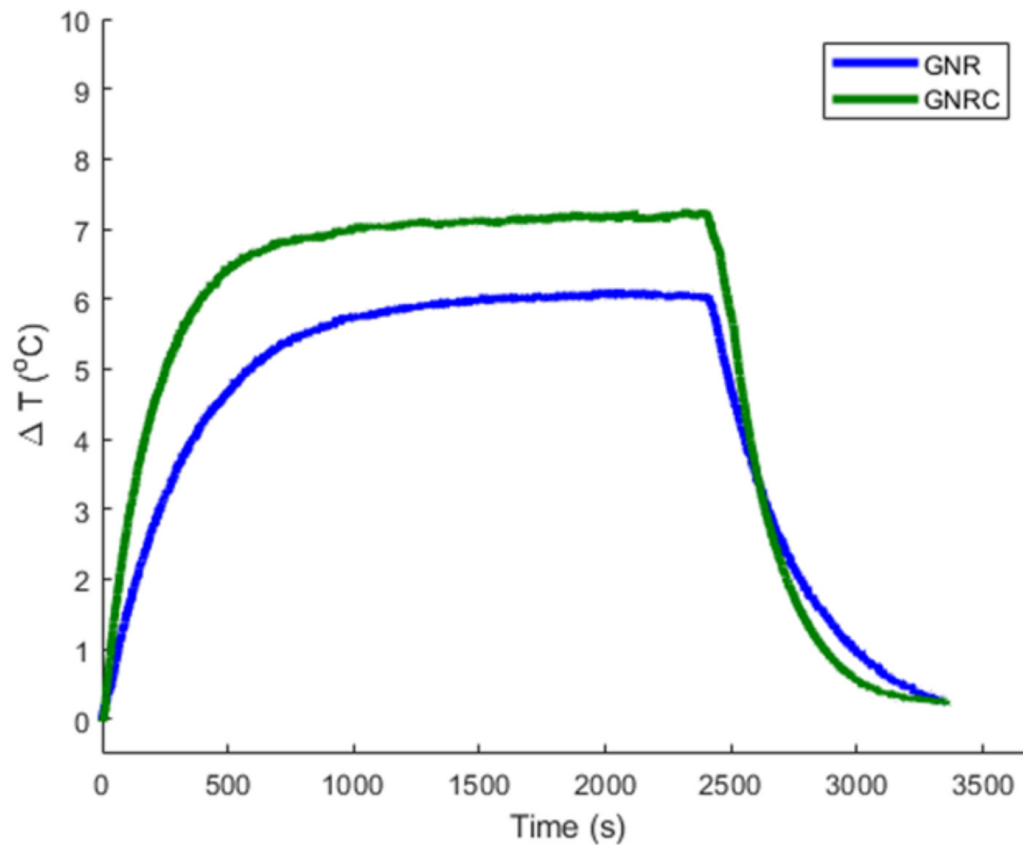
Figure 5. Heating profiles of the GNRs (blue) and GNRCs (green). The curves represent the average of 3 measurements. The maximum ΔT for the GNRs and GNRCs is 6.12 and 7.28 °C, respectively.
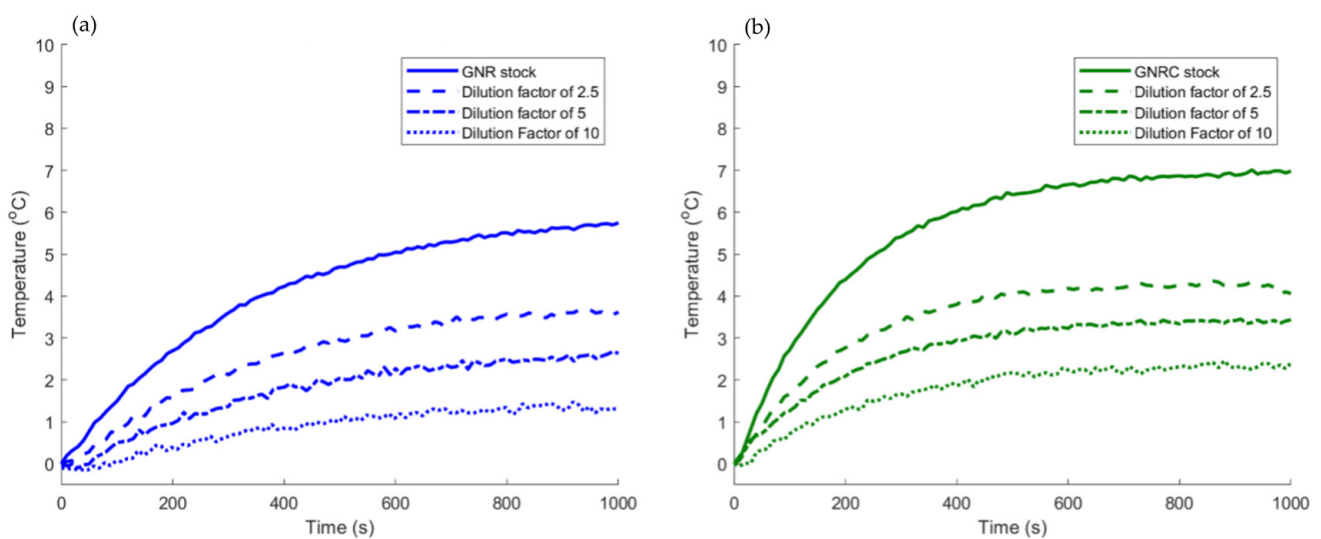
Figure 6. Concentration dependent measurements for (**a**) GNR dilutions and (**b**) GNRC dilutions. The samples were diluted by a factor of 2.5, 5, and 10. As expected, the max temperature achieved for both samples decreased as the concentration of gold decreased.
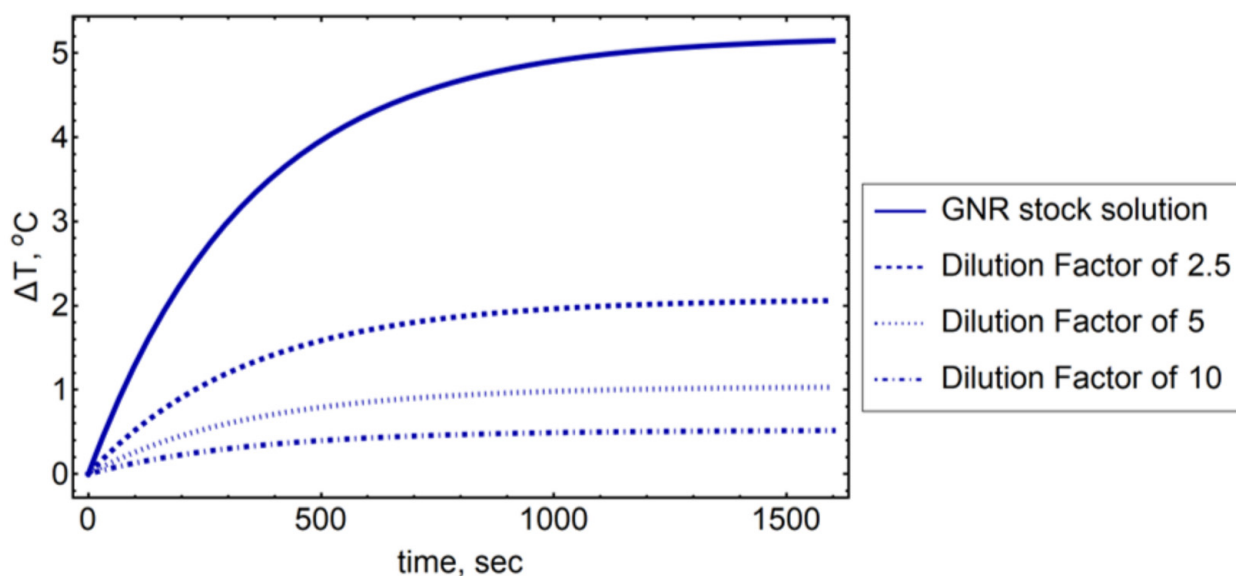
Figure 7. Theoretical temperature curves for the dilutions of the stock solution. The Q_{in} value decreased in accordance with the decrease in concentration, leading to the concentration dependent heating curves. Again, the theoretical values match well with the experimental values.

4. Discussion

In this work, we demonstrated that, not only are LED light sources an effective alternative to high-powered lasers, but also that the addition of an IR dye to the surface of gold nanorods increases their overall effectiveness. The complementary effect presented by such a conjugated IR-dye has not been previously reported and could introduce novel ways of enhancing the heating capabilities of gold nanoparticles. The heating rate of the GNRCs was found to be 63.4% higher than the GNRs, which demonstrates that rods functionalized with the IR dye allow for fast and efficient heating. This matches with previous work from our lab where Alrahili et al. [14] showed that spheres conjugated with this dye also heated faster and more efficiently than their unconjugated counterparts when exposed to a high-power laser. When considering eventual clinical application of low-power LEDs in photothermal therapy, the nanorods did heat a sufficient amount to trigger cell death—which occurs 6 °C above the standard body temperature at 43 °C as reported by Kim [27]—heating about 7 °C overall. To further strengthen this claim, we must also recognize that when allowed to circulate through the body of a patient, the tumor-targeting capabilities of the NIR-dye, shown by Usama [16], Tan [17], Luo [18], C. Zhang [19], E. Zhang [20] and Zhao [21], would allow for locally high concentrations of these nanoparticles to accumulate in and around cancer cells. This, in turn, could potentially increase the magnitude of observed heating, as was demonstrated in our dilution experiments. An additional approach to achieving larger heating effects and better understanding the role of each parameter would be to further optimize experimental conditions by exploring various LED power ranges, optical densities of the solutions, distances from the source, and various solvents. Photothermal therapy for cancer treatment using plasmonic nanomaterials has been hindered by the lack of targeting capabilities, as well as the use of unsafe lasers. However, this work opens the door for continued exploration of alternative cancer therapy options using low-powered, safe, and user-friendly LED light sources.

Author Contributions: Collected and analyzed the data presented in the manuscript and wrote the majority of the manuscript, K.C.; Performed with the theoretical calculations and provided guidance in the discussion of the theoretical results, V.S.; Provided general project guidance and help to critically review the manuscript, A.O.P.; Oversaw the project and critically reviewed and revised the manuscript, K.M. All authors have read and agreed to the published version of the manuscript.

Funding: The research presented in this manuscript was partially supported by the UCCS BioFrontiers Center (grant number: 01-2021).

Data Availability Statement: Data for the study are available upon request.

Acknowledgments: The authors would also like to thank Guy Hagen and Janusz Mankiewicz for the use of their equipment during the study, as well as Lahjavida (Colorado Springs, CO, USA) for supplying the dye conjugated gold nanoparticles under study.

Conflicts of Interest: The authors declare no conflict of interest.

Appendix A
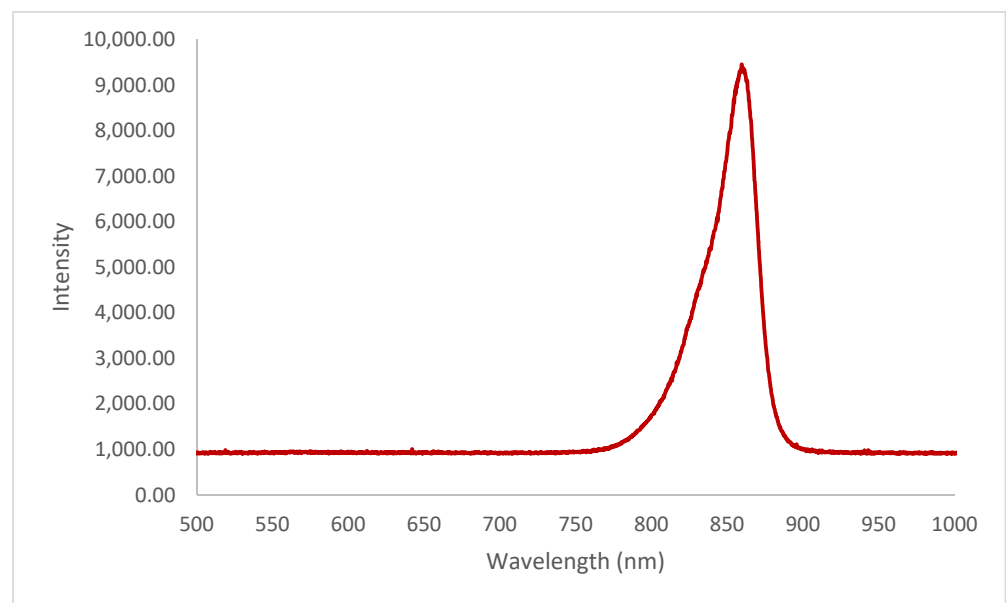
Figure A1. Emission spectrum of the light emitted diode (LED) used in heating experiments.
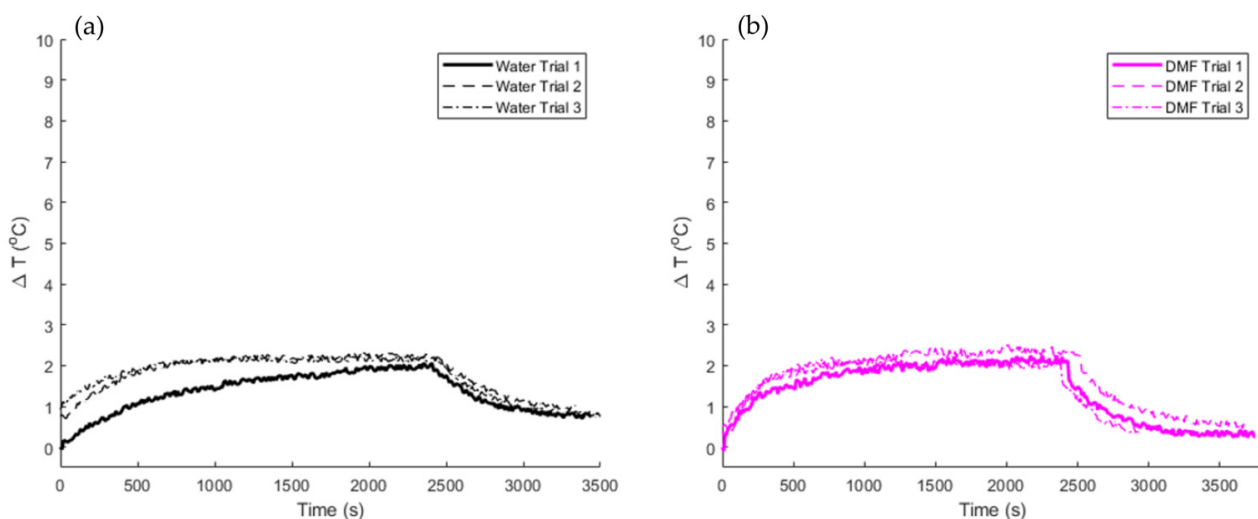
Figure A2. Heating profiles for (**a**) water and (**b**) DMF when irradiated with the 850 nm LED. The GNRs and GNRCs were dissolved in water and DMF, respectively. These temperature changes are much smaller than that observed in either of the gold nanorod solutions.
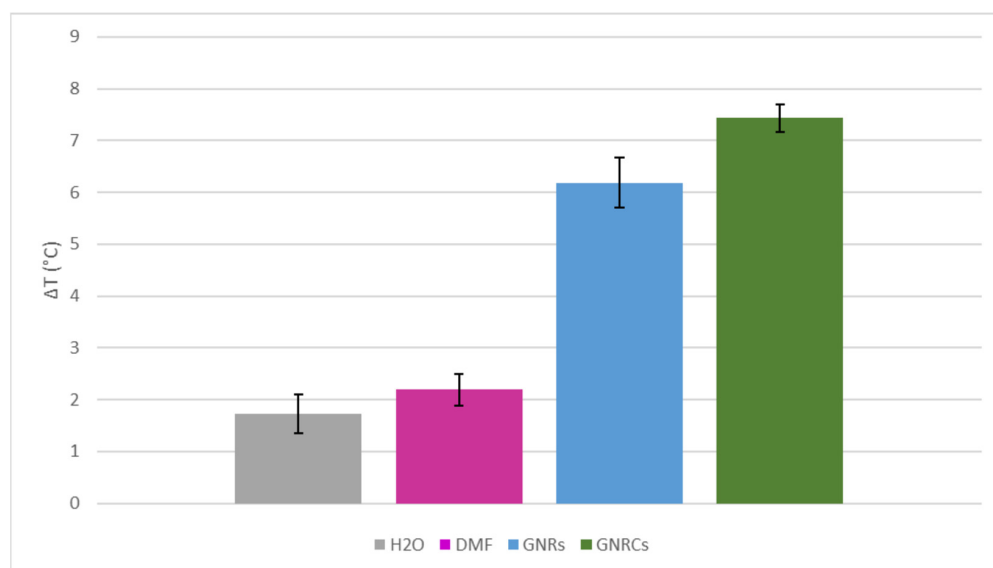
Figure A3. Average change in temperature (ΔT) for solvents and samples. The GNR sample was in H₂O and the GNRC sample was in DMF. Error bars are presented for the standard deviation between three experiments.

References

1. Centers for Disease Control and Prevention. Division of Cancer Prevention and Control, Cancer. 2021. Available online: https://www.cdc.gov/cancer/dcpc/data/index.htm (accessed on 11 October 2021).
2. Mayo Clinic, Mayo Foundation for Medical Education and Research (MFMER). 2020. Available online: https://www.mayoclinic.org/diseases-conditions/cancer/in-depth/cancer-survivor/art-20045524 (accessed on 11 October 2021).
3. Yabroff, K.R.; Mariotto, A.; Tangka, F.; Zhao, J.; Islami, F.; Sung, H.; Sherman, R.L.; Henley, S.J.; Jemal, A.; Ward, E.M. Annual Report to the Nation on the Status of Cancer, Part 2: Patient Economic Burden Associated With Cancer Care. *JNCI J. Natl. Cancer Inst.* **2021**, *113*, 1670–1682. [CrossRef] [PubMed]
4. Lee, T.; Mendhiratta, N.; Sperling, D.; Lepor, H. Focal laser ablation for localized prostate cancer: Principles, clinical trials, and our initial experience. *Rev. Urol.* **2014**, *16*, 55–66. [PubMed]
5. Wenger, H.; Yousuf, A.; Oto, A.; Eggener, S. Laser ablation as focal therapy for prostate cancer. *Curr. Opin. Urol.* **2014**, *24*, 236–240. [CrossRef] [PubMed]
6. Rosenberg, C.; Puls, R.; Hegenscheid, K.; Kuehn, J.; Bollman, T.; Westerholt, A.; Weigel, C.; Hosten, N. Laser ablation of metastatic lesions of the lung: Long-term outcome. *Am. J. Roentgenol.* **2009**, *192*, 785–792. [CrossRef]
7. Costello, A.J.; Bowsher, W.G.; Bolton, D.M.; Braslis, K.G.; Burt, J. Laser ablation of the prostate in patients with benign prostatic hypertrophy. *Br. J. Urol.* **1992**, *69*, 603–608. [CrossRef]
8. American Cancer Society. How Lasers Are Used to Treat Cancer. 2020. Available online: https://www.cancer.org/treatment/treatments-and-side-effects/treatment-types/lasers-in-cancer-treatment.html (accessed on 16 August 2022).
9. Pramanik, A.; Chavva, S.R.; Fan, Z.; Sinha, S.S.; Nellore, B.P.V.; Ray, P.C. Extremely high two-photon absorbing graphene oxide for imaging of tumor cells in the second biological window. *J. Phys. Chem. Lett.* **2014**, *5*, 2150–2154. [CrossRef]
10. Maestro, L.M.; Haro-González, P.; del Rosal, B.; Ramiro, J.; Caamano, A.J.; Carrasco, E.; Juarranz, A.; Sanz-Rodríguez, F.; Solé, J.G.; Jaque, D. Heating efficiency of multi-walled carbon nanotubes in the first and second biological windows. *Nanoscale* **2013**, *5*, 7882–7889. [CrossRef]
11. Zhou, F.; Da, X.; Ou, Z.; Wu, B.; Resasco, D.E.; Chen, W.R. Cancer photothermal therapy in the near-infrared region by using single-walled carbon nanotubes. *J. Biomed. Opt.* **2009**, *14*, 021009. [CrossRef]
12. Quintanilla, M.; Zhang, Y.; Liz-Marzán, L.M. Subtissue Plasmonic Heating Monitored with CaF₂:Nd³⁺,Y³⁺ Nanothermometers in the Second Biological Window. *Chem. Mater.* **2018**, *30*, 2819–2828. [CrossRef]
13. Jiang, K.; Smith, D.A.; Pinchuk, A. Size-dependent photothermal conversion efficiencies of plasmonically heated gold nanoparticles. *J. Phys. Chem. C* **2013**, *117*, 27073–27080. [CrossRef]
14. Alrahili, M.; Peroor, R.; Savchuk, V.; McNear, K.; Pinchuk, A. Morphology Dependence in Photothermal Heating of Gold Nanomaterials with Near-Infrared Laser. *J. Phys. Chem. C* **2020**, *124*, 4755–4763. [CrossRef]
15. Alrahili, M.; Savchuk, V.; McNear, K.; Pinchuk, A. Absorption cross section of gold nanoparticles based on nir laser heating and thermodynamic calculations. *Sci. Rep.* **2020**, *10*, 18790. [CrossRef] [PubMed]
16. Usama, S.M.; Zhao, B.; Burgess, K. A Near-IR Fluorescent Dasatinib Derivative That Localizes in Cancer Cells. *Bioconjug. Chem.* **2019**, *30*, 1175–1181. [CrossRef] [PubMed]

17. Tan, X.; Luo, S.; Wang, D.; Su, Y.; Cheng, T.; Shi, C. A NIR heptamethine dye with intrinsic cancer targeting, imaging and photosensitizing properties. *Biomaterials* **2012**, *33*, 2230–2239. [CrossRef]

18. Luo, S.; Zhang, E.; Su, Y.; Cheng, T.; Shi, C. A review of NIR dyes in cancer targeting and imaging. *Biomaterials* **2011**, *32*, 7127–7138. [CrossRef]

19. Zhang, C.; Liu, T.; Su, Y.; Luo, S.; Zhu, Y.; Tan, X.; Fan, S.; Zhang, L.; Zhou, Y.; Cheng, T. A near-infrared fluorescent heptamethine indocyanine dye with preferential tumor accumulation for in vivo imaging. *Biomaterials* **2010**, *31*, 6612–6617. [CrossRef]

20. Zhang, E.; Luo, S.; Tan, X.; Shi, C. Mechanistic study of IR-780 dye as a potential tumor targeting and drug delivery agent. *Biomaterials* **2014**, *35*, 771–778. [CrossRef]

21. Zhao, X.; Zhao, H.; Wang, S.; Fan, Z.; Ma, Y.; Yin, Y.; Wang, W.; Xi, R.; Meng, M. A Tumor-Targeting Near-Infrared Heptamethine Cyanine Photosensitizer with Twisted Molecular Structure for Enhanced Imaging-Guided Cancer Phototherapy. *J. Am. Chem. Soc.* **2021**, *143*, 20828–20836. [CrossRef]

22. Schüppert, M.; Bunge, C.-A. 5Gb/s eye-safe LED-based SI-POF transmission with equalization of transmitter nonlinearities. *IEEE Photonics Technol. Lett.* **2016**, *28*, 2732–2735. [CrossRef]

23. You, J.; Cao, D.; Hu, T.; Ye, Y.; Jia, X.; Li, H.; Hu, X.; Dong, Y.; Ma, Y.; Wang, T. Novel Norrish type I flavonoid photoinitiator for safe LED light with high activity and low toxicity by inhibiting the ESIPT process. *Dye. Pigment.* **2021**, *184*, 108865. [CrossRef]

24. Jauffred, L.; Samadi, A.; Klingberg, H.; Bendix, P.M.; Oddershede, L.B. Plasmonic Heating of Nanostructures. *Chem. Rev.* **2019**, *119*, 8087–8130. [CrossRef] [PubMed]

25. Jain, P.K.; Lee, K.S.; El-Sayed, I.H.; El-Sayed, M.A. Calculated Absorption and Scattering Properties of Gold Nanoparticles of Different Size, Shape, and Composition: Applications in Biological Imaging and Biomedicine. *J. Phys. Chem. B* **2006**, *110*, 7238–7248. [CrossRef] [PubMed]

26. He, G.S.; Zhu, J.; Yong, K.-T.; Baev, A.; Cai, H.-X.; Hu, R.; Cui, Y.; Zhang, X.-H.; Prasad, P.N. Scattering and Absorption Cross-Section Spectral Measurements of Gold Nanorods in Water. *J. Phys. Chem. C* **2010**, *114*, 2853–2860. [CrossRef]

27. Kim, M.; Kim, G.; Kim, D.; Yoo, J.; Kim, D.-K.; Kim, H. Numerical Study on Effective Conditions for the Induction of Apoptotic Temperatures for Various Tumor Aspect Ratios Using a Single Continuous-Wave Laser in Photothermal Therapy Using Gold Nanorods. *Cancers* **2019**, *11*, 764. [CrossRef]